Available online at www.sciencedirect.com
ScienceDirect
Trans. Nonferrous Met. Soc. China 29(2019) 1975−1982
Transactions of Nonferrous Metals Society of China
www.tnmsc.cn

Local corrosion mechanism of SiO_2-based refractories caused by slag movement near solid–liquid–gas interface in different slag systems

Zhang-fu YUAN, Shan-shan XIE, Xiang-tao YU, Yan-gang ZHANG, Rong-yue WANG

Collaborative Innovation Center of Steel Technology,
University of Science and Technology Beijing, Beijing 100083, China

Received 5 January 2019; accepted 31 May 2019

Abstract: Slag movement on SiO_2-based prism refractories in different slag systems was observed. The cross section shape evolution mechanism was discussed. Two types of shape evolution appear. For PbO−SiO_2 slag whose surface tension improves with SiO_2 concentration, slag film flows up along four edges under axial Marangoni shear force and wettability. Then, it flows down along four lateral faces under gravity. Corrosion rate at edges is larger than that on lateral faces due to different SiO_2 solubilities of ascending and descending flow. Prism cross section shape changes from square to round. For Fe_tO−SiO_2 slag whose surface tension reduces with the increase of SiO_2 concentration, slag film flows up under the inflence of wettability. Then, it flows down under Marangoni shear force and gravity. Compared to four edges, slag is mainly up and down on four lateral faces due to larger surface tension and size. So, prism cross section shape keeps square.

Key words: Marangoni convection; slag film; local corrosion; solid−liquid−gas interface; SiO_2-based refractories

1 Introduction

The refractory has been extensively applied in high temperature smelting industry, including ferrous industry and non-ferrous industry [1−4]. However, during the smelting process, the refractory is easily damaged due to local corrosion [5,6]. The corrosion of the refractory not only changes the composition of the slag, resulting in the reduction of the product quality, but also brings serious security issues [7]. Therefore, it is significant to investigate the local corrosion mechanism of the refractory, and further put forward corresponding measures to prevent the corrosion.

Generally, the local corrosion of the refractory occurs mainly at the refractory−slag−air (i.e., SLG) interface [8−10]. Marangoni convection is formed due to the presence of the surface tension gradient which is caused by concentration gradient, temperature gradient or composition change near the SLG interface [11,12]. And the dissolved mass transfer coefficient of slag with Marangoni convection is three times stronger than that observed in the slag under static condition [6]. Hence, Marangoni convection is an important factor for the local corrosion of the refractory. On the other hand, the local corrosion rates of different parts of the refractory material differ in different slag systems, which would lead to different shape evolution of the refractory material [13−15]. MUKAI et al [13] studied the shape evolution of SiO_2-based prism in PbO−SiO_2 slag. In our previous study, the shape evolution of SiO_2-based prism in Fe_tO−SiO_2 slag was investigated [14], and the corresponding theoretical calculation mode for different shape evolutions of the prism in the two slag systems were established based on the Laplace equation [15]. However, slag movement near SLG interface for different slag systems driven by Marangoni convection is not observed in situ, and the formation mechanism of Marangoni convection during local corrosion process is unclear.

Therefore, in this work, the slag movement patterns near the SLG interface of the SiO_2-based prism for different slag systems (PbO−SiO_2 or Fe_tO−SiO_2 slag) were observed in situ. The microstructure evolution on

Foundation item: Projects (U1738101, 51804023) supported by the National Natural Science Foundation of China; Projects (FRF-TP-18-007A1, FRF-MP-18-007) supported by Fundamental Research Funds for the Central Universities, China; Project (2019M650489) supported by China Postdoctoral Science Foundation

Corresponding author: Xiang-tao YU; Tel: +86-18811348809; E-mail: xtyuipe@163.com

DOI: 10.1016/S1003-6326(19)65105-8

local corrosion area of the prism was also investigated. The mechanism of the slag movement patterns was analyzed based on the effect of wettability, gravity and Marangoni shear stress caused by surface tension gradient. And the cross section shape evolution of prism in PbO−SiO_2 and Fe_tO−SiO_2 slags was discussed based on slag film movement characteristics.

2 Experimental

Local corrosion experiments were carried out by using X-ray radiographic apparatus (MXR−160 (1×2900), Shimadzu Corporation, Japan) [16] at high temperature. The system consists of $LaCrO_3$ bar heaters, water-cooling gum seal, high purity chamber and a PID digital program controller.

In the experiment, SiO_2-based refractory with the square prism of 10 mm × 10 mm × 80 mm was chosen as specimen. Molten silicon, PbO−SiO_2 [13] and Fe_tO−SiO_2 [14] were used as slag. When the temperature reached the required value (1693, 1713, 1733 or 1753 K) in Ar atmosphere, high purity Al_2O_3 crucibles containing molten silicon, PbO−SiO_2 slag or Fe_tO−SiO_2 slag were elevated into the homogenous-temperature zone of furnace and held for 15 min. Then, SiO_2-based specimen preheated in the upper zone of furnace was inserted slowly into molten silicon, PbO−SiO_2 slag or Fe_tO−SiO_2 slag with the dipping depth about 45 mm using the X-ray radiographic apparatus. The slag movement patterns near the SLG interface of the SiO_2-based prism for different slag systems (PbO−SiO_2 or Fe_tO−SiO_2 slag) were observed by high resolution CCD camera.

In order to observe the microstructure of the refractory at solid (refractories)–liquid (molten slag) interface, the specimen was cooled together with the slag in the Al_2O_3 crucible. And then, the specimen with the slag in the crucible was cut horizontally in the local corrosion zone using a cutting machine and polished. The surface morphology of the specimen before and after corrosion was also examined by the scanning electron microscopy (SEM) (JEOL JSM−7001F). On the other hand, the specimen was extracted from the melt and then cooled, after being dipped for a certain time (0.9−15 ks). Shape evolution of local corrosion and the corrosion depth were observed with the optical microscopy. Then, local corrosion rate was measured, and the measuring method has been described elsewhere in detail [16].

3 Results and discussion

3.1 Mechanism of melt movement driven by Marangoni convection

The corrosion of refractory material is mainly caused by the melt movement near the SLG interface. The mechanism of melt movement driven by Marangoni convection was analyzed in the SiO_2-based prism refractory and molten silicon system. When the SiO_2-based prism was immersed in the molten silicon, as Fig. 1(a) shows, the SiO_2−Si(l)−air interface was formed. Due to the wettability, the molten silicon liquid firstly flowed up along the SiO_2-based prism to form a liquid film. The local corrosion of SiO_2-based prism occurred in the contact zone between prism surface and the liquid film (Fig. 1(a)). The oxygen concentration in the liquid film near the SiO_2-based prism was higher than that in the bulk of the molten silicon (C_{O1}>C_{O2}), due to the dissolution of SiO_2. According to the results of Fig. 1(b), the surface tension of molten silicon decreased gradually with the increase of oxygen concentration. Therefore, the surface tension of molten silicon at point *e* was larger than that at point *a*. This meant that there was a surface tension gradient in the molten silicon near the SiO_2-based prism, which led to the formation of Marangoni convection.

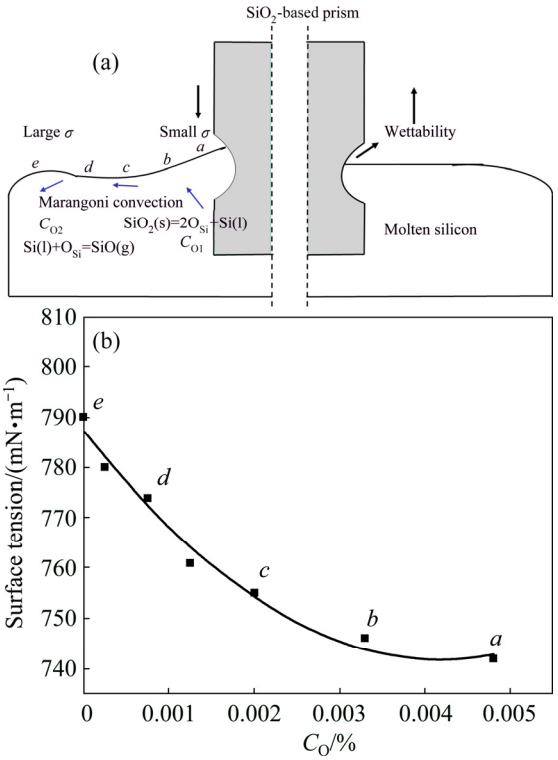

Fig. 1 Schematic diagram for movement characteristics of molten silicon near local corrosion zone of SiO_2-based prism (a) and dependence of surface tension on oxygen concentration in molten silicon (b)

The shape of the molten silicon liquid film in steady state can be expressed by the Laplace equation [13]:

$$H^2 = 2(1-\sin\theta)g^{-1}(\sigma/\rho) \quad (1)$$

where H is the height of the liquid film; g is the

gravitational acceleration; σ and ρ are the surface tension and density of the molten silicon, respectively; θ is the contact angle between the molten silicon and the SiO_2-based prism.

As shown in Fig. 1(a), the associated reactions in this system were as follows [17,18]:

$$SiO_2(s)=Si(l)+2O_{Si} \quad (2)$$

$$Si(l)+O_{Si}=SiO(g) \quad (3)$$

$$Si(l)+1/2O_2=SiO(g) \quad (4)$$

Due to the dissolution of SiO_2 (Eq. (2)), the oxygen was concentrated in the liquid film on SiO_2-based prism and transferred to the bulk of molten silicon. On the other hand, the evaporation of SiO(g) occurred in the bulk of molten silicon (Eqs. (3) and (4)). If the oxygen supply rate of SiO_2(s) was lower than the evaporation rate of SiO(g), the oxygen concentration in the bulk of molten silicon would decrease. Then, the oxygen concentration gradient would become larger, resulting in the increase of σ/ρ. According to Eq. (1), the height of the liquid film (H) increased (i.e., the SLG interface rose). At this point, the contact area between the molten silicon and SiO_2-based prism enlarged. Thus, the oxygen concentration gradient increased, leading to the intensification of Marangoni convection. Accordingly, the oxygen supply rate for molten silicon from liquid film to bulk increased. However, when the oxygen supply rate of SiO_2(s) was higher than the evaporation rate of SiO(g), the oxygen concentration in the bulk of molten silicon would increase, which would lead to the decrease of σ/ρ. Consequently, the height of liquid film (H) reduced (i.e., the SLG interface dropped). The SLG interface of molten silicon liquid film moved up and down circularly. So, the local corrosion zone near SLG interface was rapidly formed.

From the above analysis, it can be found that the effect of dissolved matter concentration on the surface tension of melt can influence the movement of melt by influencing the surface tension gradient distribution. So, in the following, the slag movement on SiO_2-based prism is investigated in two slag systems ($PbO-SiO_2$ and Fe_tO-SiO_2 slags), in which the effect of dissolved SiO_2 concentration on surface tension was different.

3.2 In-situ observation of movement patterns of different slag systems

Bubbles were adopted to clearly observe the movement pattern of the $PbO-SiO_2$ slag on the local corrosion area of the SiO_2-based prism. To observe the motion of slag film, SiO_2 was fixed at the low end of Al_2O_3 tube with Pt wire to make it consistent with the crucible center line, and the changes in the three-phase interface of SiO_2(g)−slag(l)−gas were recorded with a digital camera. As shown in Fig. 2, the bubbles moved upward at edges (indicated by the yellow circles and arrows in Fig. 2) and downward at lateral faces (indicated by the red circles and arrows in Fig. 2), respectively. It indicated that the slag film flowed up at each edge and flowed down at lateral faces in the local corrosion zone. Figure 3 shows the schematic diagram of the movement pattern for $PbO-SiO_2$ slag film in the local corrosion zone of SiO_2-based prism. As the slag film moved along the edge to the highest point, the slag flowed into two sides due to the influence of gravity. The slag gathered at each face and then flowed down to bulk (indicated by the arrows in Fig. 3).

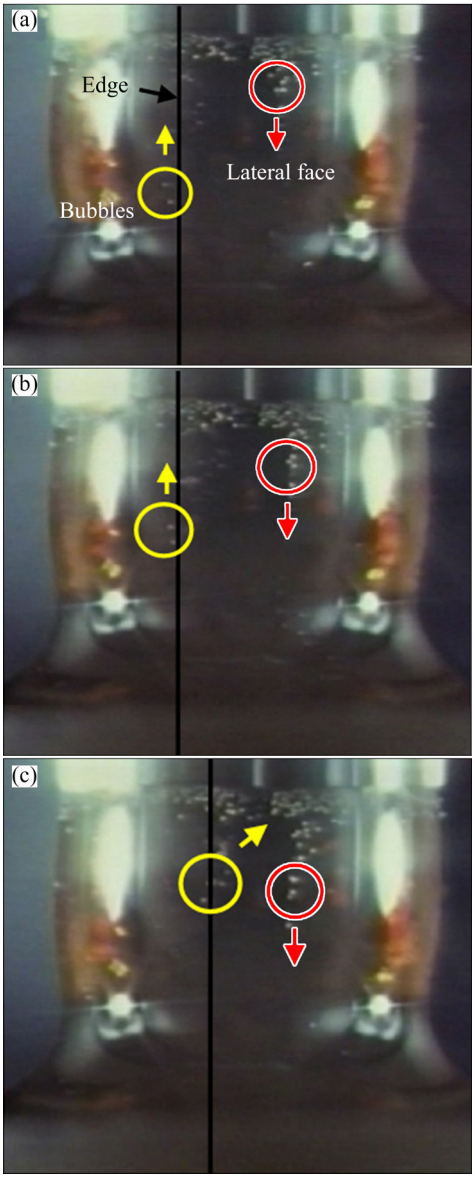

Fig. 2 Images showing movement pattern of $PbO-SiO_2$ slag in local corrosion zone of SiO_2-based prism observed by bubble tracing method: (a) 1007 s; (b) 1015 s; (c) 1026 s

By comparison, the movement pattern of the Fe_tO-SiO_2 slag on the local corrosion zone of the SiO_2-based prism was also observed in situ (Fig. 4). It

could be found that after the SLG interface of the slag film reached the highest point (Fig. 4(a)), it began to fall down to the lowest point (Figs. 4(b) and (c)). Then, the SLG interface flowed up to the highest point again (Figs. 4(d) and (e)). The movement pattern in Fe_tO−SiO_2 slag was up-and-down movement (Fig. 5), which was quite different from that in PbO−SiO_2 slag.

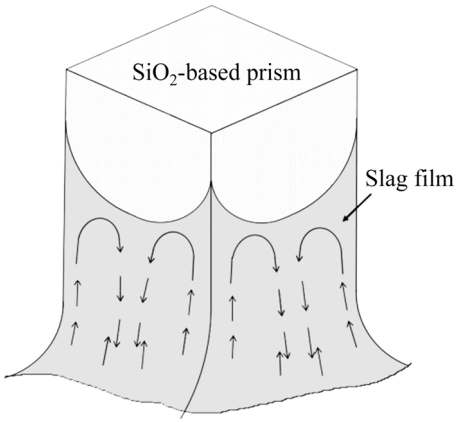

Fig. 3 Schematic diagram of movement pattern for PbO−SiO_2 slag film in local corrosion zone of SiO_2-based prism

3.3 Marangoni convection driving local corrosion mechanism in PbO−SiO_2 slag

It is well known that Marangoni convection is caused by surface tension gradient. Temperature gradient and solute concentration gradient are the main reasons for the formation of surface tension gradient. However, the movement characteristics of slag film (Figs. 2 and 4), as the main reason for the local corrosion of refractory materials, are dominated by Marangoni convection. Therefore, it is significant to clarify the formation and evolution mechanism of Marangoni convection near the SLG interface.

The SiO_2-based prisms were immersed into PbO−SiO_2 slag at different temperatures for different time. From the optical images (Fig. 6(a)), it could be found that the local corrosion mainly occurred at SLG interface, and the local corrosion became more serious with time. It was interesting that the cross section shape of SiO_2-based prisms changed from square to round after corrosion. The evolution of cross section shape might be related to the Marangoni convection characteristics in PbO−SiO_2 slag.

In order to study the corrosion process, the cross sectional microstructure of refractory−slag interface was observed (Figs. 6(b) and (c)). It could be found that a corrosion zone with many corrosion pits was formed at refractory−slag interface. From the result, it could be inferred that, the corrosion pits were formed first and then linked together, leading to the corrosion of refractory. The corrosion process was similar with that in previous works [19,20]. The thickness of corrosion zone at edge was much less than that at lateral face, which indicated that the corrosion rate at edge was much larger than that at lateral face. For SiO_2-based prisms after corrosion in PbO−SiO_2 slags at different temperatures (1693, 1713, 1733 and 1753 K), the cross section shapes were round. It was indicated that the movement pattern of PbO−SiO_2 slag film at different temperature was not changed. The linear loss representing local corrosion rate was also obtained by experiments. It was found that the linear loss increased with the increase of slag temperature (Fig. 6(d)).

For PbO−SiO_2 slag, the surface tension was improved with the increase of dissolved SiO_2 concentration [13]. It could be found from Eq. (1) that, a certain height of the slag film (H>0) was formed due to the good wettability, after the SiO_2-based prism was

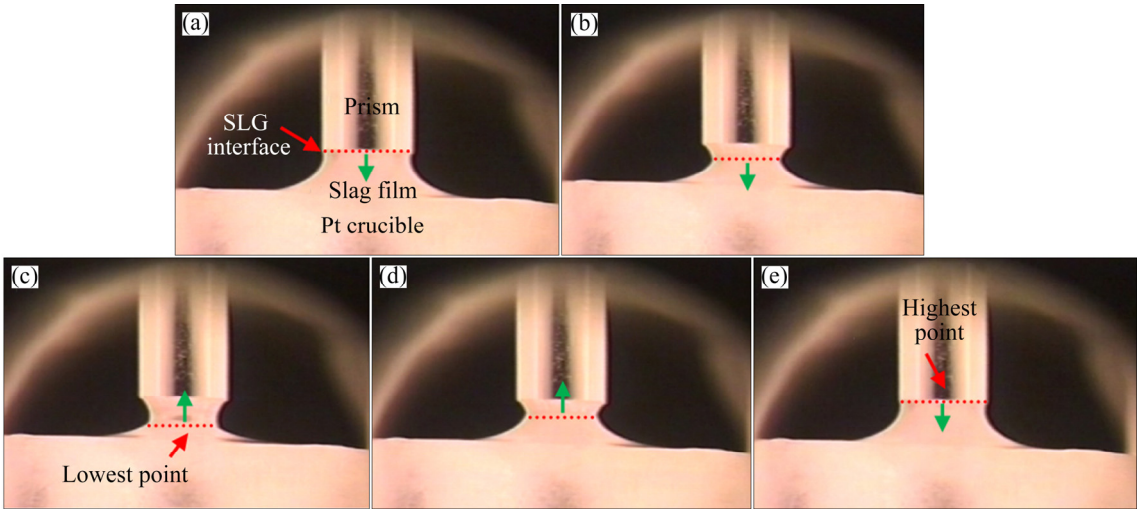

Fig. 4 Images showing movement pattern of Fe_tO−SiO_2 slag in local corrosion zone of SiO_2-based prism: (a) 3024 s; (b) 3025 s; (c) 3026 s; (d) 3028 s; (e) 3036 s

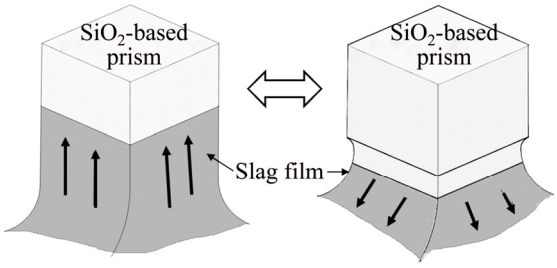

Fig. 5 Schematic diagram of movement pattern for Fe_tO−SiO_2 slag film in local corrosion zone of SiO_2-based prism

immersed in the PbO−SiO_2 slag (Figs. 7(a) and (b)). Meanwhile, due to the dissolution and diffusion of SiO_2, a SiO_2 concentration gradient formed between prism surface and slag bulk. As shown in Figs. 7(b) and (c), the SiO_2 concentration near prism surface was higher than that in slag bulk (C_1>C_{b0}, C_3>C_b). So, a radial surface tension gradient was formed near prism (σ_1>σ_{b0}, σ_3>σ_b), producing a Marangoni shear force perpendicular to tension gradient. The force caused slag film to flow up along prism. In addition, the relationship between the solubility of solid sample in melt and the curvature radius was as follows [15]:

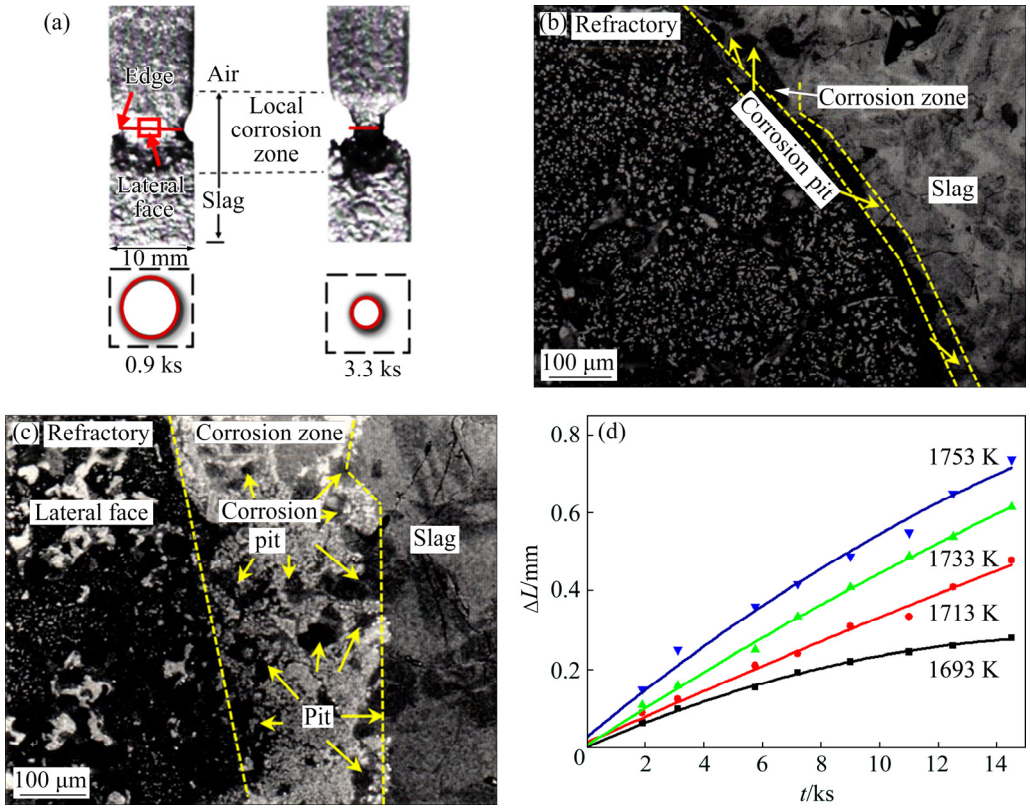

Fig. 6 Optical images of prism refractory after being immersed into PbO−SiO_2 slag for different time (a), cross sectional SEM images of refractory−slag interface at edge (b) and lateral face (c), and linear loss representing local corrosion rate of SiO_2-based prisms immersed into PbO−SiO_2 slag at different temperatures for different time (d)

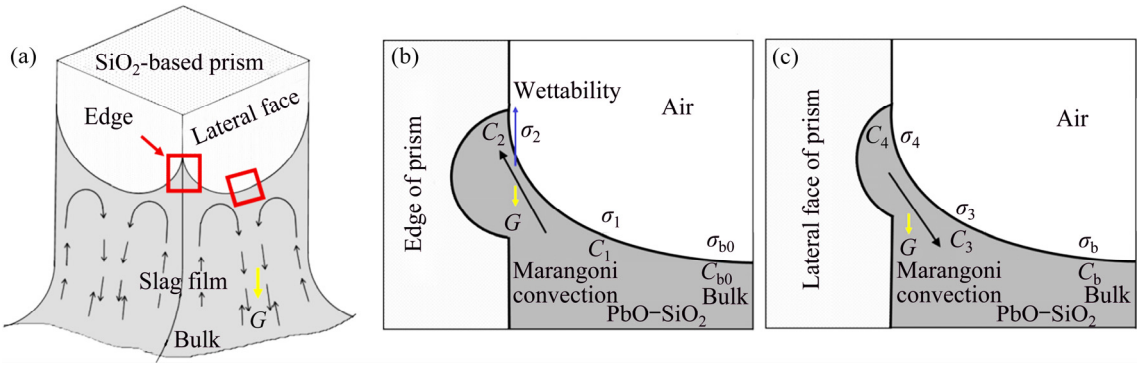

Fig. 7 Typical up-at-edge and down-at-face movement pattern of PbO−SiO_2 slag film on SiO_2-based prism (a), and cross section magnifications of edge (b) and lateral face (c)

$$\ln\frac{c_r}{c_\infty}=\frac{2M\sigma_{s-L}}{\rho_s RTr} \quad (5)$$

where c_r and c_∞ are the solubility of the solid samples with curvature radii of r and ∞ (∞ means the curvature is infinite), respectively; M and ρ_s are the relative molecular mass and density of the solid sample, respectively; σ_{s-L} is the interface tension; R and T are the gas constant and the thermodynamic temperature, respectively.

As shown in Eq. (5), the solubility (i.e., the dissolution driving force) became larger as the radius of curvature decreases. Therefore, the dissolution rate at four edges of solid prism was larger than that at four lateral faces. The SiO_2 concentration in the slag near edges was higher than that near lateral faces (C_1>C_3), which led to the fact that the surface tension of slag near edges was larger than that near lateral faces (σ_1>σ_3). As a result, the ascending flow mainly occurred at the four edges of prism. During the upward flow of slag film, the SiO_2 concentration in the upper part of liquid film was higher than that in lower part (C_2>C_1). Thus, the axial surface tension gradient was formed in the slag film due to the axial concentration gradient (σ_2>σ_1). Therefore, the radial Marangoni shear force was created, which promoted the slag film flowing aside. At the same time, under the effect of gravity, the slag liquid gathered at the highest point of edge. Then, it flowed aside and gathered on the lateral face, forming a descending flow. Finally, the up-at-edge and down-at-face movement pattern was formed (Fig. 2). Compared with the descending flow, the SiO_2 concentration in ascending flow was lower, thus leading to stronger solubility. So, the corrosion rate at four edges was larger than that at lateral faces, which was consistent with the results observed in Figs. 6(b) and (c). As a result, the cross section shape of prism was transformed from square to round (Fig. 6(a)).

3.4 Marangoni convection driving local corrosion mechanism in Fe_tO−SiO_2 slag

Different from PbO−SiO_2 slag, the surface tension of Fe_tO−SiO_2 slag decreased with the rising of dissolved SiO_2 concentration [14]. From the optical image (Fig. 8(a)), it can be found that the cross section shape of SiO_2-based prism did not change during corrosion process. Before corrosion, the surface morphology of refractory was smooth and compact (Fig. 8(b)). However, after corrosion, it became rough due to the forming of many interconnected corrosion pits (Fig. 8(c)), which was similar to the microstructure of corrosion zone in Figs. 6(b) and (c). For SiO_2-based prisms after corrosion in Fe_tO−SiO_2 slags at different temperatures (1683, 1713

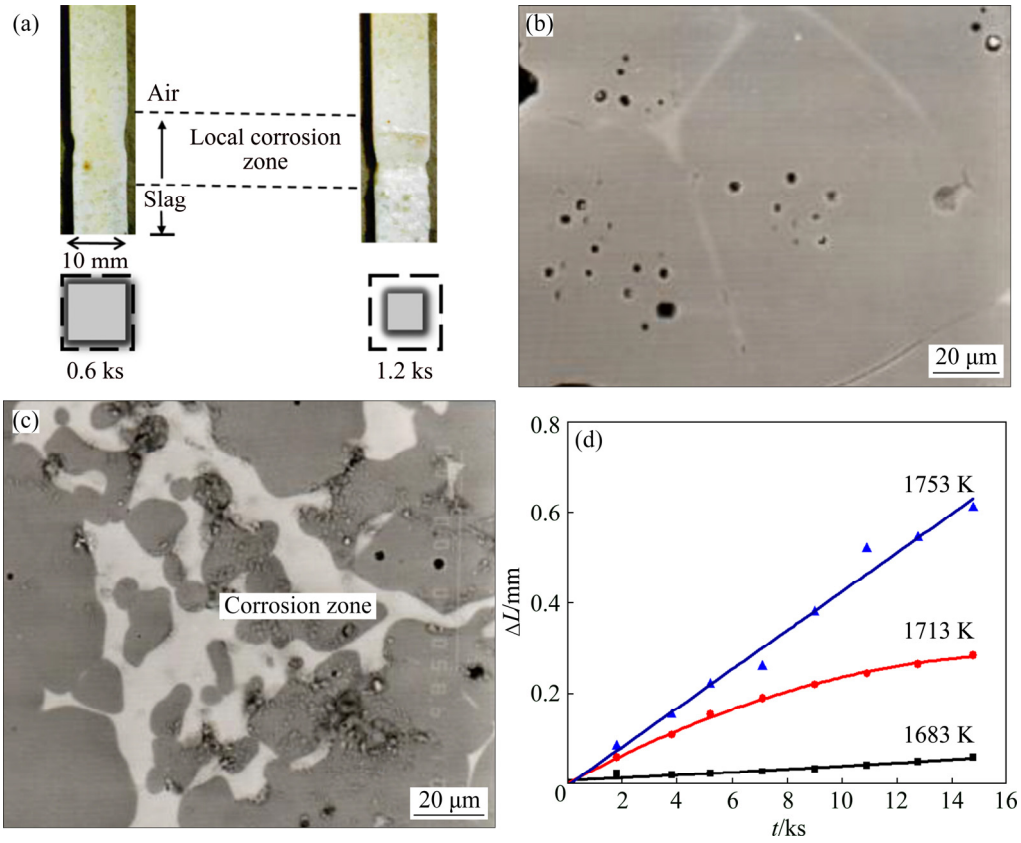

Fig. 8 Optical images of SiO_2-based prisms after being immersed into Fe_tO−SiO_2 slag for different time (a), surface morphologies of SiO_2-based prisms before corrosion (b) and after corrosion (c), and linear loss representing local corrosion rate of SiO_2-based prisms immersed into Fe_tO−SiO_2 slag at different temperatures for different time (d)

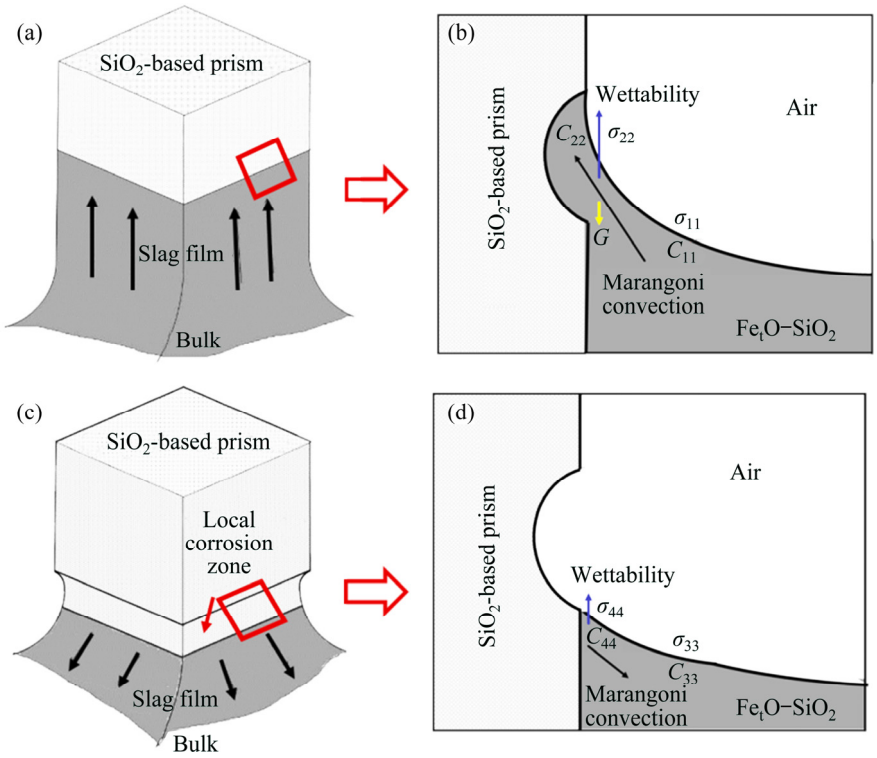

Fig. 9 Typical up-and-down movement pattern of Fe_tO−SiO_2 slag film on SiO_2-based prism (a, c) and magnification (b, d)

and 1753 K), the cross section shapes were still square, indicating the same movement pattern. It can be also found that the linear loss increased with the rising of slag temperature (Fig. 8(d)).

When the SiO_2-based prism was immersed in Fe_tO−SiO_2 slag, it can be seen from Eq. (1), the slag flowed up along the prism and reached the highest point (Figs. 9(a) and (b)). Due to the dissolution and diffusion of SiO_2, SiO_2 concentration gradient was formed between prism surface and slag bulk (C_{22}>C_{11}). So, a surface tension gradient was formed in the slag near prism (σ_{22}<σ_{11}), which caused Marangoni convection that flowed from prism surface to slag bulk. Under the influence of Marangoni convection and gravity, slag film moved downward along the prism. Simultaneously, the dissolved SiO_2 was transferred from the slag film near prism to slag bulk, due to the Marangoni convection and mass diffusion. The SiO_2 concentration in the vicinity of prism and in slag bulk would be homogenized (i.e., C_{44} is close to C_{33}). The slag liquid near prism was close to the initial state, and the slag film rose again under the influence of wettability (Figs. 9(c) and (d)). So, the up-and-down movement pattern was formed. On the other hand, as shown in Eq. (5), the dissolution rate at the lateral face was slower than that at the edge, due to the larger curvature radius. Thus, at the lateral face, the SiO_2 concentration was lower, leading to a greater surface tension. In addition, the size of four lateral faces is much larger than that of four edges. So, the up-and-down movement of slag liquid was mainly along the four lateral faces of prism, while it was relatively weak at four edges. As a result, the cross section shape of prism remained square (Fig. 8(a)).

4 Conclusions

(1) The slag movement pattern and the local corrosion of the SiO_2-based prism showed a strong dependence on the effect of dissolved SiO_2 concentration on the slag surface tension. In dependence on the Marangoni shear force determined by the surface tension gradient, two types of slag movement patterns were formed, which resulted in two different cross section shape evolution of the corroded prisms.

(2) The first type of movement patterns was the up-at-edge and down-at-face movement. The PbO−SiO_2 slag film flowed up along four edges to the highest point under upward axial Marangoni shear force. Then, the slag film flowed down along four lateral faces, under the influence of radial Marangoni shear force and gravity. The corrosion rate at the edges was larger than that at the lateral faces. As a result, the prism cross section shape changed from square to round.

(3) The other one was the up-and-down movement pattern in the Fe_tO−SiO_2 slag whose surface tension reduced with the increase of the dissolved SiO_2 concentration. The slag film rose due to the wettability effect and flowed down due to the Marangoni convection and gravity effect. The up-and-down movement of the slag liquid was mainly along the four lateral faces of the

prism, while relatively weak at the four corners. So, the cross section shape of the prism remained the original square.

References

[1] MU Wen-ning, LU Xiu-yuan, CUI Fu-hui, LUO Shao-hua, ZHAI Yu-chun. Transformation and leaching kinetics of silicon from low-grade nickel laterite ore by pre-roasting and alkaline leaching process [J]. Transactions of Nonferrous Metals Society of China, 2018, 28: 169−176.

[2] YEH Chun-liang, CHEN Yi-chang. In situ formation of $Zr_2Al_3C_4/Al_2O_3$ composites by combustion synthesis with PTFE and thermal activations [J]. Transactions of Nonferrous Metals Society of China, 2018, 28: 2011−2516.

[3] WANG Qi-yu, ZOU Xiao-dong, MATSUURA H, WANG Cong. Evolution of inclusions during the 1473 K (1200 °C) heating process of EH36 shipbuilding steel [J]. Metallurgical and Materials Transactions B, 2018, 49(1): 18−22.

[4] LI Ping, SUN Da-zhi, WANG Xue, XUE Ke-min, HUA Rui, WU Yu-cheng. Microstructure and thermal stability of sintered pure tungsten processed by multiple direction compression [J]. Transactions of Nonferrous Metals Society of China, 2018, 28: 461−468.

[5] ZOU Xiao-dong, ZHAO Da-peng, SUN Jin-cheng, WANG Cong, MATSUURA H. An integrated study on the evolution of inclusions in EH36 shipbuilding steel with Mg addition: From casting to welding [J]. Metallurgical and Materials Transactions B, 2018, 49B: 481−489.

[6] LIAN Peng-fei, HUANG Ao, GU Hua-zhi, ZOU Yong-shun, FU Lv-ping, WANG Ya-jie. Towards prediction of local corrosion on alumina refractories driven by Marangoni convection [J]. Ceramics International, 2018, 44: 1675−1680.

[7] RICHARDSON F D. Interfacial Phenomena and Metallurgical Processes [J]. Canadian Metallurgical Quarterly, 1982, 21(2): 111−119.

[8] MATSUSHITA T, WATANABE T, HAYASHI M. Thermal, optical and surface/interfacial properties of molten slag systems [J]. International Materials Reviews, 2011, 56(5−6): 287−323.

[9] LIU S, LIU Z, WANG Y, TANG J. A comparative study on the high temperature corrosion of TP347H stainless steel, C22 alloy and laser-cladding C22 coating in molten chloride salts [J]. Corrosion Science, 2014, 83(6): 396−408.

[10] WANG Hui-jun, CABALLERO R, DU Si-chen. Dissolution of MgO based refractories in $CaO−Al_2O_3−MgO−SiO_2$ slag [J]. Journal of the European Ceramic Society, 2018, 38: 789−797.

[11] SCRIVEN L, STERNLING C. The Marangoni effects [J]. Nature, 1960, 187: 186−188.

[12] WANG Min-bo, LI Rui-di, YUAN Tie-chui, CHEN Chao, ZHANG Mei, WENG Qi-gang, YUAN Ji-wei. Selective laser melting of W−Ni−Cu composite powder: Densification, microstructure evolution and nano-crystalline formation [J]. International Journal of Refractory Metals and Hard Materials, 2018, 70: 9−18.

[13] MUKAI K, HARADA T, NAKANO T, HIRAGUSHI K. Mechanism of local corrosion of solid silica at $PbO−SiO_2$ slag surface [J]. Journal of the Japan Institute of Metals and Materials, 1986, 50: 63−67.

[14] YU Z, MUKAI K. Direct Observation of the local corrosion of solid silica at the surface of liquid $Fe_tO−SiO_2$ slags [J]. Journal of the Japan Institute of Metals and Materials, 1992, 56: 1137.

[15] HUANG Wen-lai, YUAN Zhang-fu. Shape change of prism solids in different liquid systems during local corrosion [J]. Journal of Colloid & Interface Science, 2003, 267(1): 155−159.

[16] YUAN Zhang-fu, HUANG Wen-lai, MUKAI K. Local corrosion of magnesia-chrome refractories driven by Marangoni convection at the slag-metal interface [J]. Journal of Colloid & Interface Science, 2002, 253(1): 211−216.

[17] NASS M, YOUNG D, ZHANG J, OLSEN J, TRANELL G. Active oxidation of liquid silicon: Experimental investigation of kinetics [J]. Oxidation of Metals, 2012, 78(5−6): 363−376.

[18] WAGNER C. Passivity during the oxidation of silicon at elevated temperatures [J]. Journal of Applied Physics, 1958, 29(9): 1295−1297.

[19] WAN Wei-cai, XIONG Ji, LI Yu-he, TANG Qi-feng, LIANG Meng-xia. Erosion-corrosion behavior of Ti(C,N)-based cermets containing different secondary carbides [J]. International Journal of Refractory Metals and Hard Materials, 2017, 66: 180−187.

[20] TANG Wei, ZHANG Li, CHEN Yi, ZHANG Hua-dong, ZHOU Lei. Corrosion and strength degradation behaviors of binderless WC material and WC−Co hardmetal in alkaline solution: A comparative investigation [J]. International Journal of Refractory Metals and Hard Materials, 2017, 68: 1−8.

不同渣系中固–液–气界面渣运动引起的 SiO_2 基耐火材料局部熔损机理

袁章福，谢珊珊，于湘涛，张岩岗，王容岳

北京科技大学 钢铁共性技术协同创新中心，北京 100083

摘　要：观察不同渣系在 SiO_2 基棱柱状耐火材料上的渣运动，并研究棱柱状耐火材料横截面形状的演变机理。存在两种类型的形状演变。对于其表面张力随 SiO_2 浓度增加而增大的 $PbO−SiO_2$ 渣系，在轴向马兰戈尼剪切力和润湿性的作用下，渣膜沿着棱柱状耐火材料的 4 根棱边向上流；随后，在重力作用下，渣膜沿着棱柱的 4 个侧面流下；因为上升流和下降流中 SiO_2 溶解度不同，棱边的腐蚀速率大于侧面的腐蚀速率，棱柱横截面由正方形演变为圆形。对于其表面张力随 SiO_2 浓度增加而减少的 $Fe_tO−SiO_2$ 渣系，在润湿性的作用下，渣膜向上流；之后，在马兰戈尼剪切力和重力的作用下，渣膜向下流；相比于 4 个棱边，由于 4 个侧面的表面张力和尺寸较大，渣主要在 4 个侧面上下运动；因此，棱柱横截面仍然保持为正方形。

关键词：马兰戈尼对流；渣膜；局部熔损；固−液−气界面；SiO_2 基耐火材料

(Edited by Bing YANG)